Hydrogen Adsorption and Diffusion on the Anatase TiO2(101) Surface: A First-Principles Investigation

ARTICLE *in* THE JOURNAL OF PHYSICAL CHEMISTRY C · APRIL 2011

Impact Factor: 4.77 · DOI: 10.1021/jp200408v

3 AUTHORS:

Mazharul Mohammad Islam
University of Bonn
46 PUBLICATIONS **516** CITATIONS
SEE PROFILE

M. Calatayud
Pierre and Marie Curie University - Paris 6
86 PUBLICATIONS **1,808** CITATIONS
SEE PROFILE

Gianfranco Pacchioni
Università degli Studi di Milano-Bicocca
517 PUBLICATIONS **18,389** CITATIONS
SEE PROFILE

THE JOURNAL OF PHYSICAL CHEMISTRY C

ARTICLE

pubs.acs.org/JPCC

Hydrogen Adsorption and Diffusion on the Anatase TiO_2(101) Surface: A First-Principles Investigation

Mazharul M. Islam,[*,†,‡] Monica Calatayud,[§,∥] and Gianfranco Pacchioni[⊥]

[†]Institut für Physikalische und Theoretische Chemie, Universität Bonn, Wegelerstrasse 12, 53115 Bonn, Germany

[‡]Laboratoire de Physico-Chimie des Surfaces, CNRS-ENSCP (UMR # 7045), Ecole Nationale Supérieure de Chimie de Paris, Université Pierre et Marie Curie, 11 rue Pierre et Marie Curie, 75231 Paris Cedex 05, France

[§]UPMC Université Paris 06, UMR 7616, Laboratoire de Chimie Théorique, F-75005, Paris, France

[∥]CNRS, UMR 7616, Laboratoire de Chimie Théorique, F-75005, Paris, France

[⊥]Dipartimento di Scienza dei Materiali, Università degli Studi Milano-Bicocca, via R. Cozzi, 53, Milano, Italy

ABSTRACT:

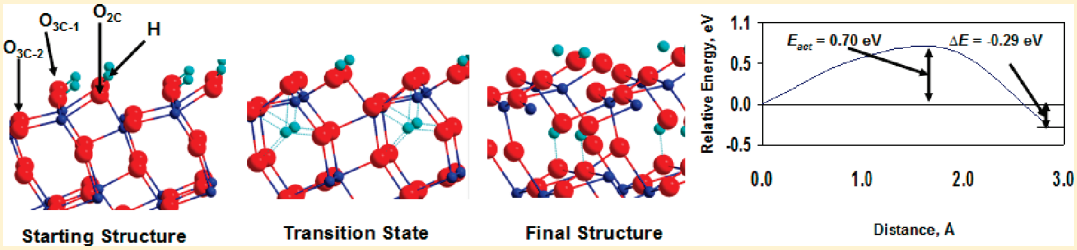

The mechanisms of adsorption of hydrogen on the anatase TiO_2(101) surface and of its diffusion in the bulk are investigated with DFT calculations and compared with similar results obtained for the diffusion of hydrogen on the rutile (110) surface. Because of the different oxygen environments in anatase and rutile surfaces, the H binding energy on the anatase surface is 0.2−0.3 eV smaller than in rutile. Various processes for H diffusion are investigated using the climbing nudged-elastic-band (cNEB) approach. We have identified three main diffusion mechanisms, leading to migration of H on the surface, diffusion into the bulk, and desorption of H_2 molecule. Our calculated activation barrier (E_{act}) shows that migration of H into the bulk is the kinetically most favorable process.

1. INTRODUCTION

Titanium dioxide, TiO_2, is one of the most intensively studied materials due to its wide range of technological and industrial applications. Unlike most other materials, TiO_2 is reactive with water but exhibits an outstanding resistance to corrosion and photocorrosion in aqueous environments. Due to these unique properties, TiO_2 has a wide range of potential environmentally friendly applications, such as photocatalytic water purification,[1−3] solar hydrogen production,[4−7] photocatalysts for self-cleaning building materials,[1] and air purification.[1]

There are four polymorphs of TiO_2 including anatase ($I4_1/amd$), rutile ($P4_2/mnm$), brookite ($Pbca$), and a high pressure phase. While rutile is thermodynamically the most stable bulk phase, most nanomaterials are in anatase form.[8] Moreover, below a particle size of ∼14 nm, the anatase phase appears to be more stable than the rutile one, which is attributed to the lower surface energy of anatase.[9,10] Anatase has the same tetragonal symmetry as rutile. The anatase structure contains four titanium and eight oxygen atoms in the unit cell with a slightly distorted TiO_6 octahedron as shown in Figure 1a.

Surface science investigations necessitate single-crystalline samples. While rutile crystals are readily available, sufficiently large and pure anatase crystals are more difficult to obtain. As anatase is a metastable phase, it transforms into rutile at relatively low temperatures,[8] with the transition temperature depending on impurities, crystal size, and sample history.

Hydrogen interaction with the TiO_2 surfaces is an important process in several phenomena and applications.[11] It has been shown that molecular hydrogen does not interact strongly with the rutile TiO_2(110) surface,[12,13] while atomic hydrogen readily sticks to the surface oxygen atoms.[14,15] Both theoretical and experimental studies indicate that rutile TiO_2 surfaces can be reduced by hydroxylation of the surface oxygen atoms via adsorption of hydrogen.[16−18] Also, the hydrogenation of anatase (001) and (100) surfaces has been reported theoretically.[19] In bulk anatase, the presence of atomic hydrogen induces the formation of Ti^{3+} centers.[20]

Our study is motivated by a recent combined experimental and DFT study of hydrogen diffusion on the rutile (110) surface.[21] In this work it was observed that hydrogen atoms diffuse into the bulk rather than desorb from the surface. In the present study, the diffusion mechanisms of hydrogen on the anatase surfaces have

Received: January 14, 2011
Revised: March 10, 2011
Published: March 22, 2011

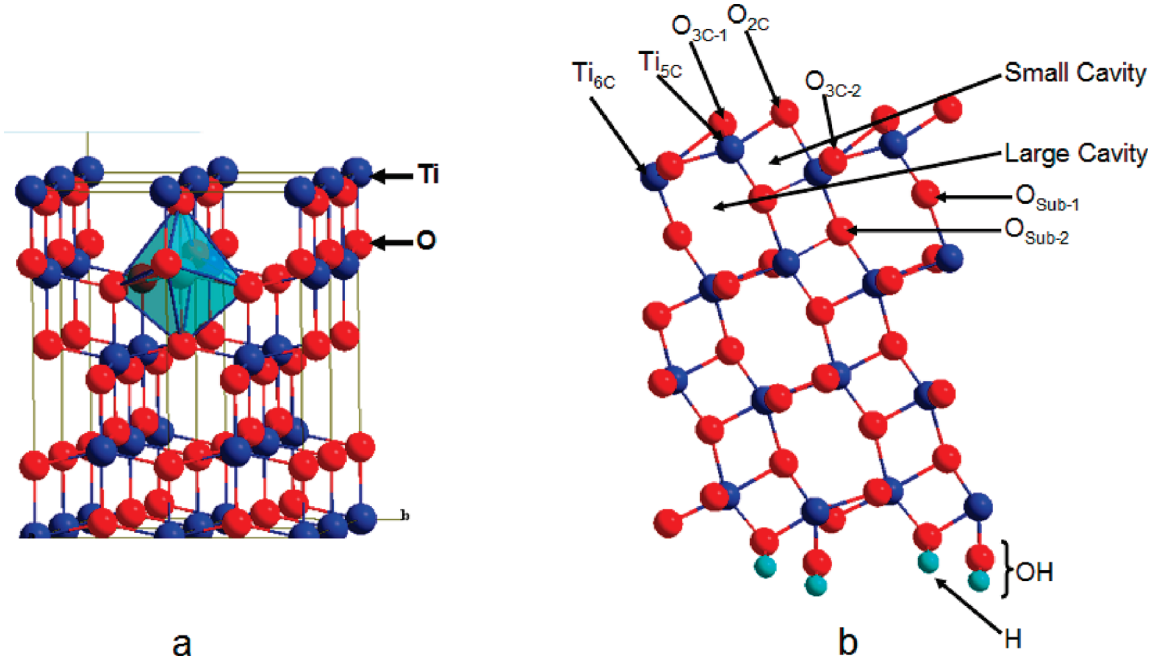

Figure 1. (a) Tetragonal crystal structure of anatase TiO_2 bulk. A 2 × 2 × 1 supercell is shown. (b) 2 × 2 supercell of the slab of anatase TiO_2(101) surface (side view). Red, deep blue, and light blue spheres represent the oxygen, titanium, and hydrogen atoms, respectively.

been investigated theoretically in a systematic way by using quantum mechanical approaches from first principles. The adsorption of hydrogen has been considered on the various possible positions at the surface and subsurface of anatase TiO_2(101). The work has been performed by using periodic DFT and DFT+U approaches as described in the next section.

2. COMPUTATIONAL METHODS AND MODELS

All the calculations were performed with the density functional theory (DFT) based on the generalized gradient approximation (GGA) of Perdew and Wang.[22] This method was used as implemented in the plane-wave program VASP.[23−25] The projector-augmented wave (PAW) potentials[26,27] were used for the core electron representation. A set of plane waves with an energy cutoff E_{cut} = 400 eV was used for valence electrons as in the case of rutile surface.[21] For comparison, hydrogen adsorption on the TiO_2 surfaces was investigated by using the DFT+U approach, where the value of U was 4 eV.[28] The convergence criteria used in this study are the same as those in the previous study performed on a rutile surface.[21] The potential energy was determined by the full quantum mechanical electronic structure until the total energy differences between the loops decrease below 10^{-4} eV. The transition state search for the diffusion and migration processes was performed with the climbing nudged-elastic-band (cNEB)[29] method as implemented in VASP. Vibrational analysis calculations were performed to verify the true local minima and saddle point character of the optimized geometries. No imaginary frequency arose for the local minima structures, whereas imaginary frequency is observed for the transition state structures.

Full optimization of the lattice parameters and fractional coordinates was performed for bulk anatase TiO_2. The converged values of the optimized lattice parameters (a and c) and Ti−O bond distances are in close agreement with the corresponding experimental values. The experimental lattice parameters obtained at 15 K are a = 3.782 Å and c = 9.502 Å, and the two apical bond lengths (1.979 Å) are greater than the other four basal bond lengths (1.932 Å).[30] The calculated lattice parameters a = 3.83 Å and c = 9.66 Å for bulk anatase are overestimated by only 1.32% and 1.70%, respectively, with respect to the experimental value. Similarly, the calculated bond lengths (Ti−O (apical) = 2.00 Å and Ti−O (basal) = 1.96 Å) agree well with the experimental values.

On the basis of the optimized structure of bulk TiO_2, a slab of the (101) surface was modeled with four Ti_2O_4 layers. A vacuum layer of 15 Å was employed to prevent spurious interactions between the repeated slabs. The surface contains 5-fold (Ti_{5c}) and 6-fold (Ti_{6c}) coordinated Ti atoms and both 2-fold- (O_{2C}) and 3-fold-coordinated oxygen atoms (O_{3C-1} and O_{3C-2}) as shown in Figure 1b. In order to improve the SCF convergence, the exposed oxygen and titanium atoms of the bottom layer are saturated by dissociated H_2O molecules, as depicted in Figure 1b. Test calculation at the pure DFT level shows that spin density arising from the unpaired electron due to H adsorption is localized on the under-coordinated Ti_{5c} atoms of the bottom layer, which slows down the SCF convergence. The hydroxylated bottom Ti_2O_4 layer was kept fixed while the three top layers are relaxed during the optimization.

3. RESULTS AND DISCUSSION

3.1. Adsorption of H on the Anatase TiO_2(101) Surface. The adsorption of atomic hydrogen was investigated by placing the H atom on different surface sites in a (1 × 1) unit cell, modeling high hydrogen coverage. The surface sites considered are the 2-fold-coordinated O_{2C}, 3-fold-coordinated O_{3C-1} and O_{3C-2}, and subsurface O_{Sub-1} and O_{Sub-2}. The existence of different O_{3C} and O_{Sub} oxygen atoms is related to different O−Ti bond distances, as explained in Table 1. No matter where the H atom sits, there is always a charge transfer of one electron per H atom to the TiO_2 sample with formation of a proton H^+

Table 1. Optimized O−Ti and O−H Distances (Å) for Different Surface and Subsurface Oxygen Atoms

bonds	O_{2C}	$O_{3C\text{-}1}$	$O_{3C\text{-}2}$	$O_{Sub\text{-}1}$	$O_{Sub\text{-}2}$
O − Ti1	1.99	2.05	2.01	1.92	2.27
O − Ti2	2.25	2.05	2.23	2.58	2.11
O − Ti3		2.53	2.01	2.25	2.18
O − H	0.98	0.99	0.99	0.99	0.99

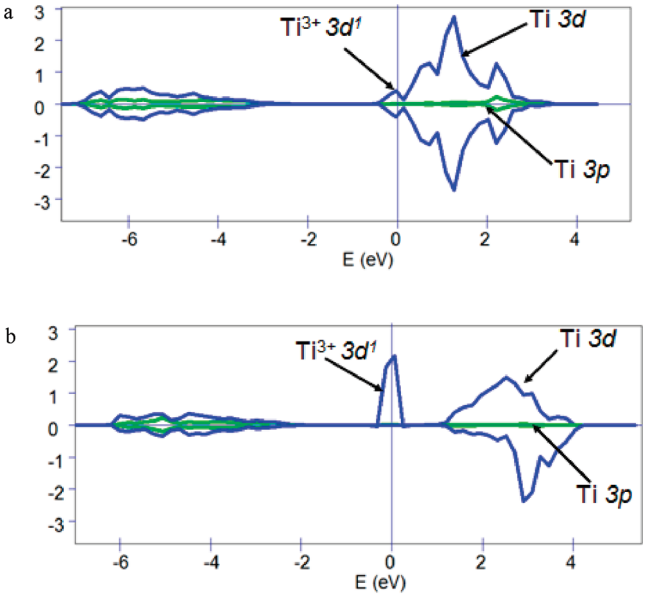

Figure 2. PDOS of Ti 3d and 3p states obtained at the GGA (a) and GGA+U level (b). The localized $Ti^{3+}3d^1$ state is marked by an arrow.

bound to an O atom and one electron that is transferred to the empty Ti 3d states, as found experimentally.[11] This can be clearly visualized by the density of states (DOS) curves. As an example, we discuss the partial DOS of Ti states for the hydrogen adsorption on the O_{2C} site in Figure 2. In GGA calculations, the electronic levels (Ti^{3+} $3d^1$) that arise from this charge transfer are at the bottom of the conduction band (as shown in Figure 2a), an effect that is related to the well-known underestimation of the band gap with this computational approach. In fact, standard DFT functionals are unable to properly describe the localization of these electrons. The self-interaction error causes an excessive repulsion between electrons in localized states, often resulting in an excessive delocalization.[31−33] At the GGA+U level, the picture is different since the Ti^{3+} $3d^1$ states are now below the bottom of the conduction band (see Figure 2b), indicating a more pronounced localization. Of course, the level of localization and the broadening of the Ti^{3+} $3d^1$ levels is also a function of the H coverage. At the high coverage considered here, indeed we observe the formation of a broad band.

The binding energy E_b for the hydrogen bound to different surface sites is calculated as,

$$E_b = (E_{Slab} + E_H) - E_{H/Slab} \quad (1)$$

where E_{Slab} and $E_{H/Slab}$ are the energies of the slabs without and with hydrogen adsorbed on the surface, respectively, and E_H is the energy of atomic hydrogen (−1.115 eV). The calculated E_b for the anatase (101) surfaces are compiled in Table 2 along with those obtained for the rutile (110) surface.[21] Our DFT results reveal that single H atoms adsorb preferentially on top of the bridging 2-fold coordinated oxygen atoms (O_{2C}) similar to the rutile (110) surface. The next preferred adsorption site is $O_{Sub\text{-}2}$, followed by the 3-fold-coordinated oxygen site $O_{3C\text{-}2}$. We have also considered pairs of H atoms resulting from the dissociation of an H_2 molecule, and we find that adsorption on O_{2C} and $O_{Sub\text{-}2}$ is the most stable among all considered coadsorption sites.

Table 2. Comparison of Calculated Adsorption Energies, E_b (eV), for Hydrogen Adsorption on the Anatase (101) and Rutile (110) Surfaces

	anatase (101)		rutile (110)	
types	DFT	DFT+U	DFT[a]	DFT+U
1 H: O_{2C}	2.31	2.35	2.52	2.50
1 H: $O_{Sub\text{-}2}$	2.04	1.90	2.34	1.87
1 H: $O_{3C\text{-}2}$	1.65	1.85	1.76	1.83
1 H: $O_{Sub\text{-}1}$	1.37			
1 H: $O_{3C\text{-}1}$	1.33			
2 H: O_{2C}+$O_{Sub\text{-}1}$	1.10			
2 H: O_{2C}+$O_{Sub\text{-}2}$	1.53	1.82	1.88	
2 H: O_{2C}+$O_{3C\text{-}1}$	1.02			
2 H: O_{2C}+$O_{3C\text{-}2}$	1.15	1.56	1.54	
2 H: $O_{3C\text{-}2}$+$O_{Sub\text{-}1}$	1.35			
2 H: $O_{3C\text{-}2}$+$O_{Sub\text{-}2}$	1.44	1.75		

[a] Reference 21.

Although the general trend of the nature of hydrogen adsorption and the calculated E_b values on the anatase (101) and rutile (110) surfaces are similar, the absolute values of E_b for anatase are always smaller than those for the rutile surface.

The H adsorption energy is on the order of 2.30 eV on the most stable site (for comparison, adsorption on anatase (100) is reported to be 2.32 eV and on (001) it is of 1.56 eV).[19] Since the H_2 dissociation costs 4.54 eV in experiment[34] and 4.39 eV in GGA, the global adsorption of H_2 on the anatase surface is nearly thermoneutral (actually slightly exothermic). This holds true for both rutile and anatase surfaces. The results are not too different if instead of a pure GGA functional we use the GGA+U approach. This is true in particular for the preferred adsorption site where the differences between the two functionals are of the order of a few hundreds of an electron volt (Table 2). Also the trend in stability of hydrogen binding on various surface and subsurface oxygen atoms obtained with the DFT and DFT+U methods is the same. Therefore, in the next section, the transition state search calculations for the hydrogen migration using the NEB approach are performed only at the GGA level.

3.2. Mechanisms of Hydrogen Migration on the Anatase TiO_2(101) Surface. The migration of hydrogen on the anatase (101) surface was investigated assuming that a H_2 molecule has dissociated and that one of the two resulting H atoms moves around while the second one remains fixed. Initial combinations of sites are O_{2C}H+$O_{3C\text{-}1}$H, $O_{3C\text{-}1}$H+$O_{3C\text{-}2}$H, and O_{2C}H+$O_{3C\text{-}2}$H. We have considered migration paths of the H atom from the $O_{3C\text{-}1}$, O_{2C}, and $O_{3C\text{-}2}$ sites when O_{2C}, $O_{3C\text{-}1}$, and O_{2C}, respectively, are hydroxylated. Hydrogen can migrate through either a small cavity or a large cavity (as illustrated in Figure 1b). All the migration pathways appear to overcome an activation barrier

Table 3. Calculated Energy, Activation Barriers E_{act} (eV), and Energy Difference between Intitial and Final Structures ΔE (eV) for Atomic Hydrogen Diffusion on the Anatase (101) Surface (See Also Figures 3 and 4)

	position of H				
migration type	starting model	transition state	final model	E_{act}	ΔE
Migration 1	$O_{2C} + O_{3C\text{-}1}$	$O_{3C\text{-}1} + O_{3C\text{-}2}$	$O_{3C\text{-}1} + (O_{3C\text{-}2}+O_{Sub})$	2.25	0.98
Migration 2	$O_{2C} + O_{3C\text{-}1}$	$O_{2C} + O_{Sub}$	$O_{2C} + O_{Sub}$	0.70	− 0.29
Migration 3	$O_{3C\text{-}2} + O_{2C}$	$O_{2C} + (O_{3C\text{-}2}+O_{3C\text{-}1})$	$O_{2C} + O_{Sub}$	2.05	− 0.13
Migration 4	$O_{3C\text{-}1} + O_{3C\text{-}2}$	$O_{2C} + O_{3C\text{-}2}$	$O_{2C} + O_{3C\text{-}2}$	1.41	− 0.71
Migration 5	$O_{2C} + O_{3C\text{-}1}$	$O_{2C} + (O_{3C\text{-}1}+O_{3C\text{-}2})$	$O_{2C} + O_{3C\text{-}2}$	1.35	− 0.12
Migration 6	$O_{2C} + O_{3C\text{-}2}$	O_{2C}	H_2	2.06	− 0.95

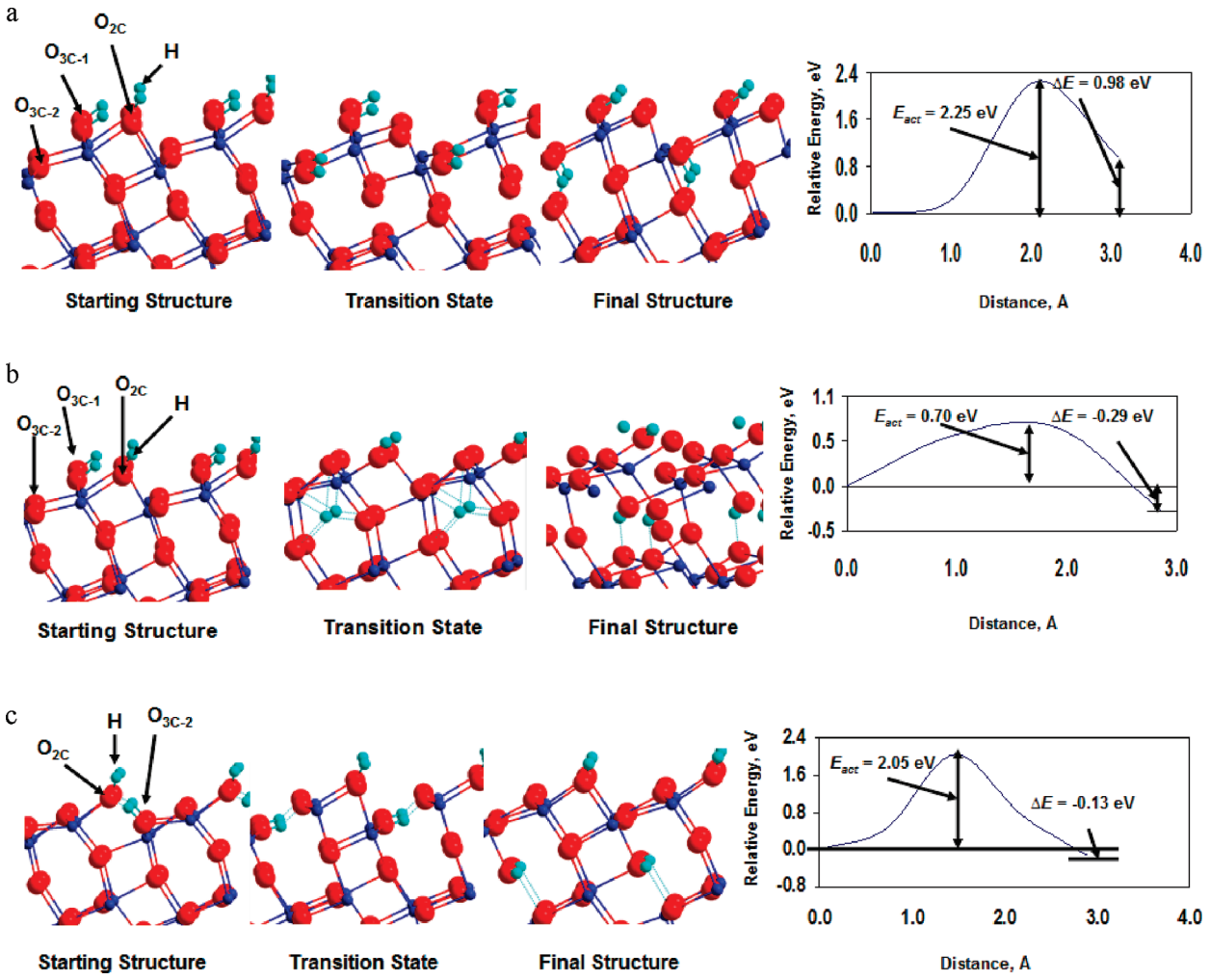

Figure 3. Diffusion of hydrogen atoms into the bulk through large cavity. Only the upper layers of 2 × 2 supercell are shown. (a) Migration 1: H migration from O_{2C} when $O_{3C\text{-}1}$ is hydroxylated; (b) Migration 2: H migration from $O_{3C\text{-}1}$ when O_{2C} is hydroxylated; (c) Migration 3: H migration from $O_{3C\text{-}2}$ when O_{2C} is hydroxylated.

E_{act}. The migration through the small cavity results in surface diffusion or desorption of an H_2 molecule, whereas the migration through large cavity results in H diffusion into the bulk. These migration paths are described in detail below. ΔE is the energy difference between the final state and initial state (Table 3).

3.2.1. Diffusion of H into the Bulk. To estimate the activation energy required for subsurface migration, three migration pathways have been investigated. These are: migration of H from O_{2C} when $O_{3C\text{-}1}$ is bound to H (Migration 1), migration of H from $O_{3C\text{-}1}$ when O_{2C} is bound to H (Migration 2), and migration of H from $O_{3C\text{-}2}$ when O_{2C} is bound to H (Migration 3). As mentioned above, these diffusions occur through the large cavity.

The path for Migration 1 is reported in Figure 3a, where the starting, transition state, and final structures are shown. It is interesting to note the structural changes during the H migration process. In the starting model, both O_{2C} and $O_{3C\text{-}1}$ are in hydroxyl

dx.doi.org/10.1021/jp200408v |J. Phys. Chem. C 2011, 115, 6809–6814

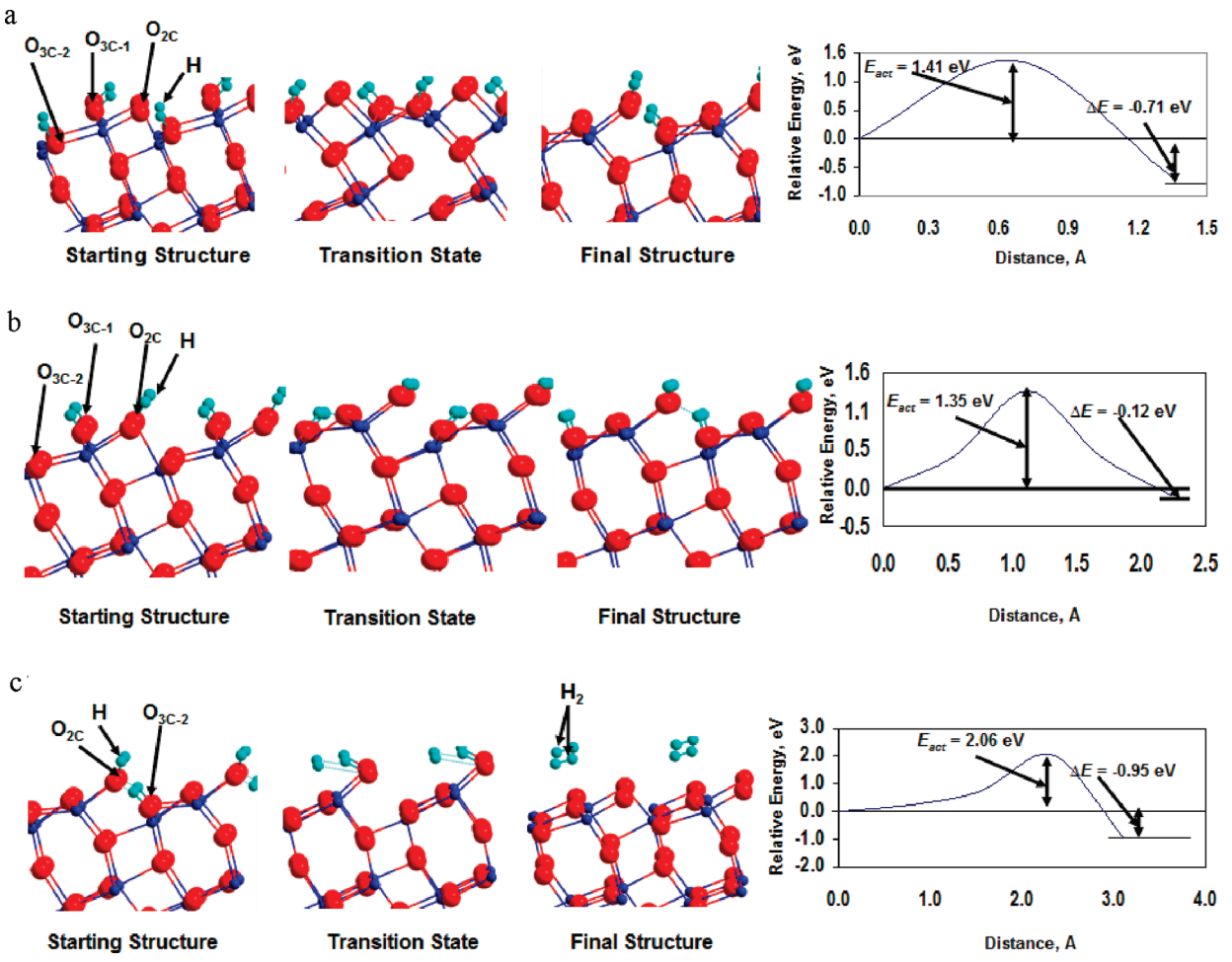

Figure 4. (a) Migration 4: Diffusion on the surface where H migrates from $O_{3C\text{-}1}$ to O_{2C} (through small cavity) with hydroxylated $O_{3C\text{-}2}$; (b) Migration 5: H diffusion on the surface where H migrates from $O_{3C\text{-}1}$ to $O_{3C\text{-}2}$ with hydroxylated O_{2C}; (c) Migration 6: Direct desorption via formation of H_2 molecule. Only the upper layers of the 2 × 2 supercell are shown.

form with an O−H bond of 0.99 Å. In the transition state, one H migrates from O_{2C} to $O_{3C\text{-}2}$, indicating a surface migration. In the final structure, one H is attached to $O_{3C\text{-}1}$, whereas the second H is attached to $O_{3C\text{-}2}$ with a partial bond with the subsurface oxygen atom. The activation barrier (E_{act}) is 2.25 eV (Figure 3a). The energy difference (ΔE) between the final and initial structures of this migration process is +0.98 eV. This shows that the final structure is highly unstable compared to the initial model.

In the second diffusion process (Migration 2, Figure 3b), one H is always bound to O_{2C}, whereas the second H migrates from $O_{3C\text{-}1}$ to the subsurface region to form a bond with the O_{Sub} (1.00 Å). In this process, the activation barrier of H migration is 0.70 eV only, indicating that H diffusion to the subsurface region is favorable and can occur even below room temperature. The calculated ΔE is −0.29 eV, showing that the final model is more stable than the starting structure, and that diffusion into the bulk is a thermodynamically spontaneous process. In the third diffusion process (Migration 3, Figure 3c), one H is always bound to O_{2C}, whereas the second H migrates from $O_{3C\text{-}2}$ to the subsurface region through a large cavity. In the transition structure, the migrating H forms bonds with $O_{3C\text{-}2}$ (1.01 Å) and $O_{3C\text{-}1}$ (1.53 Å), whereas in the final structure it forms a bond with the subsurface oxygen O_{Sub} with bond distance of 0.98 Å. In this process, the activation barrier (E_{act}) is high (2.05 eV). Also in this case, the final structure is more stable than the initial one with a ΔE = −0.13 eV. However, the high barrier makes this process rather unlikely.

3.2.2. Migration of H on the Surface. Diffusion of H through a small cavity results in H migration on the surface. The most likely surface migration pathway corresponds to the migration of H from $O_{3C\text{-}1}$ when $O_{3C\text{-}2}$ is in OH form. This is named Migration 4 (see Figure 4a). It is observed that the migrating H does not diffuse into the subsurface region but rather diffuses on the surface. In fact, in the starting structure, H is bound to $O_{3C\text{-}1}$ (0.98 Å) and $O_{3C\text{-}2}$ (0.99 Å), whereas in the final structure H is bound to $O_{3C\text{-}2}$ (1.01 Å) and O_{2C} (0.97 Å). The calculated activation barrier (E_{act}) for such a migration pathway is 1.41 eV, i.e., is 0.7 eV larger than diffusion of H into the bulk (see previous paragraph). The calculated ΔE is −0.71 eV, indicating that this migration process is thermodynamically favorable. Therefore, it is possible that at finite temperatures a number of events involve H diffusion on the surface before migration into the bulk takes place. This is in agreement with the results of Table 3 regarding the stability of bridging O_{2C}−H groups. O_{2C} would always be hydrogenated, and surface migration will rather involve $O_{3C\text{-}1}$ to/from $O_{3C\text{-}2}$.

This process is further checked by performing a direct migration of H from $O_{3C\text{-}1}$ to $O_{3C\text{-}2}$ when O_{2C} is always in OH form. This migration path is denoted as Migration 5 and illustrated in

dx.doi.org/10.1021/jp200408v |J. Phys. Chem. C 2011, 115, 6809–6814

Figure 4b. In this process, E_{act} is 1.35 eV and is similar to that of the Migration 4 process. Also in this case, the final structure is more stable than the initial one with $\Delta E = -0.12$ eV.

3.2.3. Desorption of H_2 Molecule. We have investigated the recombination of two surface OH groups leading to desorption of the H_2 molecule. Therefore, we have performed a direct desorption study via formation of H_2 (see Migration 6, Figure 4c). Here the initial structure of the cNEB process contains two H atoms on O_{2C} and $O_{3C\text{-}2}$, whereas in the final structure a H_2 molecule desorbs from the surface. The activation barrier (E_{act}) for this migration process is 2.06 eV, while the computed ΔE is −0.95 eV, showing that, in this case, the final structure is very stable compared to the initial one.

On the basis of the calculated activation barriers (Table 3) for the various migration processes, we conclude that migration of H into the bulk (Migration 2, E_{act} = 0.70 eV, $\Delta E = -0.29$ eV) is kinetically the most favorable process. Diffusion of H on the surface (Migration 5, E_{act} = 1.35 eV, $\Delta E = -0.12$ eV) is the second most likely mechanism for the H migration. On the other hand, hydrogen desorption via formation of H_2 is kinetically difficult although thermodynamically possible (Migration 6, E_{act} = 2.06 eV, $\Delta E = -0.95$ eV).

4. SUMMARY AND CONCLUSIONS

Hydrogen interaction and diffusion on the anatase TiO_2(101) surface have been investigated by systematic quantum-chemical DFT calculations. Various surface and subsurface oxygen sites were chosen for the study of H adsorption. The results suggest that single H atoms adsorb preferentially on top of the bridging 2-fold coordinated oxygen atom (O_{2C}); this is similar to what happens on the rutile (110) surface where the preferred adsorption site is also an O_{2C}. The next adsorption site in terms of stability is the subsurface site ($O_{Sub\text{-}2}$). For pairs of H atoms, coadsorption on O_{2C} and $O_{Sub\text{-}2}$ is the most stable among all considered sites. The DOS curves show that the unpaired electrons are always localized on Ti 3d orbitals giving rise to electronic states in the gap below the bottom of the conduction band.

Various mechanisms of H migration were investigated, and the transition state has been identified using the cNEB approach. Our study reveals that there are three competing processes, namely, migration of H on the surface, diffusion of H into the bulk, and desorption of H_2 molecule. By comparing the calculated activation barriers, we conclude that the most likely mechanism is the diffusion of H into the bulk since this is both kinetically and thermodynamically favorable.

AUTHOR INFORMATION

Corresponding Author

*E-mail: rana-islam@thch.uni-bonn.de.

ACKNOWLEDGMENT

M.M.I. is grateful to the COST D36 and D41 Actions for making possible his stay at the University of Milano Bicocca. This work was performed using HPC resources from GENCI-CINES/IDRIS (Grant x2010081548) and the CCRE-DSI of Université P. M. Curie.

REFERENCES

(1) Fujishima, A., Hashimoto, K., Watanabe, T. *TiO_2 Photocatalysis. Fundamentals and Applications*; BKC, Inc.: Tokyo, 1999; pp 14−176.
(2) Linsebigler, A. L.; Lu, G.; Yates, J. T., Jr. *Chem. Rev.* **1995**, *95*, 735.
(3) Ryu, J.; Choi, W. *Environ. Sci. Technol.* **2008**, *42*, 294.
(4) Fujishima, A.; Honda, K. *Nature* **1972**, *238*, 37.
(5) Nowotny, J.; Bak, T.; Nowotny, M. K.; Sheppard, L. R. *Int. J. Hydrogen Energy* **2007**, *32*, 2609.
(6) Nowotny, J.; Bak, T.; Nowotny, M. K.; Sheppard, L. R. *J. Phys. Chem. C* **2008**, *112*, 5275.
(7) Tang, J.; Durrant, J. R.; Klug, D. R. *J. Am. Chem. Soc.* **2008**, *130*, 13885.
(8) Ranade, M. R.; Navrotsky, A.; Zhang, H. Z.; et al. *Proc. Natl. Acad. Sci. U.S.A.* **2002**, *99*, 6476.
(9) Lazzeri, M.; Vittadini, A.; Selloni, A. *Phys. Rev. B* **2001**, *63*, 155409.
(10) Amores, J. M. C.; Escribano, V. S.; Busca, G. *J. Mater. Chem.* **1995**, *5*, 1245.
(11) Panayotov, A. D.; Yates, J. T. *Chem. Phys. Lett.* **2007**, *436*, 204.
(12) Henrich, V. E.; Kurtz, R. L. *Phys. Rev. B* **1981**, *23*, 6280.
(13) Kunat, M.; Burghaus, U.; Wöll, Ch. *Phys. Chem. Chem. Phys.* **2004**, *6*, 4203.
(14) Suzuki, S.; Fukui, K. I.; Onishi, H.; Iwasawa, Y. *Phys. Rev. Lett.* **2000**, *84*, 2156.
(15) Fujino, T.; Katayama, M.; Inudzuka, K.; Okuno, T.; Oura, K. *Appl. Phys. Lett.* **2001**, *79*, 2716.
(16) Kowalski, P. M.; Meyer, B.; Marx, D. *Phys. Rev. B* **2009**, *79*, 115410.
(17) Leconte, J.; Markovits, A.; Skalli, M. K.; Minot, C.; Belmajdoub, A. *Surf. Sci.* **2002**, *497*, 194.
(18) Bouzoubaa, A.; Markovits, A.; Calatayud, M.; Minot, C. *Surf. Sci.* **2005**, *583*, 107.
(19) Calatayud, M.; Minot, C. *Surf. Sci.* **2004**, *552*, 169.
(20) Di Valentin, C.; Pacchioni, G.; Selloni, A. *J. Phys. Chem. C* **2009**, *113*, 20543.
(21) Yin, X.-L.; Calatayud, M.; Qiu, H.; Wang, Y.; Brikner, A.; Minot, C.; Wöll, Ch. *ChemPhysChem* **2008**, *9*, 253.
(22) Perdew, J. P.; Wang, Y. *Phys. Rev. B* **1992**, *45*, 13244.
(23) Kresse, G.; Hafner, J. *Phys. Rev. B* **1993**, *47*, 558.
(24) Kresse, G.; Hafner, J. *Phys. Rev. B* **1993**, *48*, 13115.
(25) Kresse, G.; Hafner, J. *Phys. Rev. B* **1994**, *49*, 14251.
(26) Kresse, G.; Joubert, J. *Phys. Rev. B* **1999**, *59*, 1758.
(27) Blöchl, P. E. *Phys. Rev. B* **1994**, *50*, 17953.
(28) Finazzi, E.; Di Valentin, C.; Pacchioni, G.; Selloni, A. *J. Chem. Phys.* **2008**, *129*, 154113.
(29) Jónsson, H.; Mills, G.; Jacobsen, K. W. In *Classical and Quantum Dynamics in Condensed Phase Simulations*; Berne, B. J., Ciccotti, G., Coker, D. F., Eds.; World Scientific: Singapore, 1998; p 385.
(30) Burdett, J. K.; Hughbanks, T.; Miller, G. J.; Richardson, J. W.; Smith, J. V. *J. Am. Chem. Soc.* **1987**, *109*, 3639.
(31) Cohen, A. J.; Mori-Sanchez, P.; Yang, W. *Science* **2008**, *321*, 792.
(32) Di Valentin, C.; Pacchioni, G.; Selloni, A. *Phys. Rev. Lett.* **2006**, *97*, 166803.
(33) Di Valentin, C.; Pacchioni, G.; Selloni, A. *J. Phys. Chem. C* **2009**, *113*, 20543.
(34) *CRC Handbook of Chemistry and Physics*, 89th ed.; Taylor and Francis: Boca Raton, FL, 2009.